Plasma Sources Science and Technology

PAPER • **OPEN ACCESS**

On the quasi-stationary approach to solve the electron Boltzmann equation in pulsed plasmas

To cite this article: A Tejero-del-Caz *et al* 2021 *Plasma Sources Sci. Technol.* **30** 065008

OPEN ACCESS
IOP Publishing
Plasma Sources Science and Technology
Plasma Sources Sci. Technol. **30** (2021) 065008 (15pp)
https://doi.org/10.1088/1361-6595/abf858

On the quasi-stationary approach to solve the electron Boltzmann equation in pulsed plasmas

A Tejero-del-Caz[1,2], V Guerra[1], N Pinhão[1], C D Pintassilgo[1,3] and L L Alves[1,*]

[1] Instituto de Plasmas e Fusão Nuclear, Instituto Superior Técnico, Universidade de Lisboa, Av. Rovisco Pais, 1049-001 Lisboa, Portugal
[2] Departamento de Física, Facultad de Ciencias, Universidad de Córdoba, Campus de Rabanales, 14071 Córdoba, Spain
[3] Departamento de Engenharia Física, Faculdade de Engenharia, Universidade do Porto, R. Dr. Roberto Frias, 4200-465 Porto, Portugal

E-mail: llalves@tecnico.ulisboa.pt

Received 1 May 2020, revised 30 March 2021
Accepted for publication 15 April 2021
Published 8 June 2021

Abstract

This work analyzes the temporal evolution of the electron kinetics in dry-air plasmas (80% N_2: 20% O_2), excited by electric-field pulses with typical rise-times of 10^{-9} and 10^{-6} s, applied to a stationary neutral gaseous background at pressures of 10^5, 133 Pa and temperature of 300 K. The study is based on the solution of the electron Boltzmann equation (EBE), adopting either (i) a time-dependent formulation that considers an intrinsic time evolution for the electron energy distribution function (EEDF), assuming the classical two-term expansion and a space-independent exponential temporal growth of the electron density; or (ii) a quasi-stationary approach, where the time-independent form of the EBE is solved for different values of the reduced electric-field over the duration of the pulse. The EBE was solved using the LisbOn KInetics Boltzmann solver (LoKI-B), whose original capabilities were extended to accept time-dependent non-oscillatory electric fields as input data. The role of electron–electron collisions, under specific conditions, is also reported and discussed. The simulations show that the quasi-stationary approach gives solutions similar to the time-dependent formulation for rise-times longer than the characteristic evolution time of the EEDF, i.e. 20 ns at 10^5 Pa and 20 μs at 133 Pa, meaning that a quasi-stationary description is possible in a high-collisionality situation and long rise-times (e.g. microsecond pulses at atmospheric pressure), failing for faster rise-times (e.g. nanosecond pulses for both pressures considered here).

Keywords: low-temperature plasmas, electron kinetics, fast-pulsed discharges, Boltzmann solver, LoKI-B

(Some figures may appear in colour only in the online journal)

* Author to whom any correspondence should be addressed.

1. Introduction

Recently, there has been increasing interest in non-equilibrium low-temperature plasmas (LTPs) created by pulsed discharges, because of their potential advantages in different technological applications [1], such as nanosecond pulsed discharges for plasma-assisted ignition and combustion, as pointed out in [2] and reviewed in detail in [3, 4]. Among other specific characteristics, the typical time of production of active species in nanosecond plasma discharges is shorter than that of ignition and combustion. In addition, the use of pulsed plasmas brings the advantage of low power and high-energy efficiency in the production of active species and electronically excited states [5]. For these reasons, nanosecond pulsed discharges have been studied in a large variety of gases, including pure N_2 [6], air [7–11], N_2–O_2 [12], N_2–H_2 [13], and even more complex mixtures such as H_2–air [14], C_2H_4–air [15] and hydrocarbon–air [16]. The principles of plasma-assisted combustion and ignition have been also recommended for plasma chemical-conversion [17], involving dry reforming or plasma pyrolysis and management of CO_2. Within this line of research, the study of nanosecond pulsed discharges has been extended for example to CO_2 [18, 19], CH_4 [20, 21] and CH_4–CO_2 mixtures [22, 23]. With respect to fast-pulsed plasmas, it is also worth noting the very intense research developed recently with the purpose to measure their electric field [24–28].

Behind these applications is the fact that changing the voltage applied to gases at intermediate-to-high pressures, during the nanosecond to microsecond time-scale typical of breakdown, greatly affects the plasma parameters and composition. With the advent of non-equilibrium plasmas at atmospheric pressures for many applications, discharges generated by voltage pulses with rise times up to hundreds of volts per nanosecond (or even higher) have become promising environments to tune the plasma for each specific application [1]. In this context, global models represent a simple, yet powerful, tool to study and understand plasmas produced by (fast-)pulsed discharges. Their self-consistent solution requires information on the electron macroscopic parameters (rate coefficients and transport parameters), which can be obtained by coupling the chemistry solver to an electron Boltzmann equation (EBE) solver, often written in the classical two-term approximation.

The analysis of the electron kinetics as a function of time has been addressed by several authors in the past. A survey of the investigation on this subject was presented by Winkler and Wilhelm already in 1979 [29], and in subsequent years the group of Greifswald continued to actively pursue this line of research, for example proposing a numerical method to solve the non-stationary two-term EBE and analysing the temporal evolution of the electron energy distribution function (EEDF) and the main macroscopic quantities in neon, for great perturbations of the electric field by a rectangular pulse [30]; by developing hybrid methods, coupling the non-stationary two-term EBE with discharge models as reviewed in [31], to self-consistently describe different time-dependent systems, such as pumped plasmas for excimer lasers [32], the temporal decay of the diffusion-controlled afterglow of a positive column [33], and more recently pulsed air-like low-pressure dc plasmas [34]. The subject received contributions also from other authors and groups, for example to study homogeneous plasmas excited by time-varying sinusoidal electric-fields, by solving the Fourier-development in time of the two-term EBE, analysing the influence of electron-vibrational excitations/deexcitations in N_2 and H_2 plasmas at various oscillating frequencies [35] and the time evolution of the first excited states of argon in high-frequency (HF) plasmas [36]; to follow the time evolution of the EEDF in the nitrogen afterglow, by solving the time-dependent EBE [37], also coupled to the equations ruling the time evolution of the heavy-particles (including the vibrational distribution function (VDF)) [38]; to analyse the diffusion of electrons in time-dependent $E \times B$ fields by using Monte Carlo simulations [39, 40]; to monitor the temporal or the spatiotemporal electron relaxation, by using the solution of the two-term/multi-term expansion of the EBE and Monte Carlo simulations, in argon plasmas [41, 42], argon–fluorine decaying plasmas due to the unbalance between the electron attachment and ionisation rates [43], and the nanosecond breakdown in atmospheric air [44]. Time-dependent algorithms were used also to solve the two-term EBE (even when the goal was to obtain a stationary solution), as illustrated for example in [45] that presents the 1D modelling of a helium glow discharge based on the solution of the time- and space-dependent EBE.

Note that some of the previous works [6, 13, 32–34, 36, 38, 45] already include the coupling of models describing the time-dependent kinetics of electrons and heavy-particles, with particular focus on the mutual influence between the EEDF and the VDF of molecules, later extended to the kinetics of electronically excited states. This line of work was initiated in the 1980s by the groups of Bari and Greifswald that published extensive literature on the subject, of which we will only mention (as an example) the seminal works of Capitelli, Wilhelm and co-workers [46–53] and the very recent works of Colonna *et al* [13, 54], on the electron kinetics of active plasmas and afterglows, produced in different molecular gases by direct-current, radio-frequency, microwave and nanosecond repetitive discharges.

Despite these efforts, the coupling between Boltzmann and chemistry models continuous to assume some approximations regarding the description in time, possibly also due to the EBE solvers freely available: introducing effective source terms that account for the electron-impact creation of excited species [55], or considering a quasi-stationary description for electrons [10, 56] by solving a time-independent form of the EBE for chosen values of the reduced electric field, E/N (the ratio of the electric-field amplitude to the gas density), over the duration of the pulse. Indeed, most of the publicly available tools for solving the EBE [57–62] are limited to a stationary description, valid for LTPs excited by direct-current (DC) electric fields. Other solvers like BOLSIG+ [63, 64], EEDF [65] and LoKI-B [66, 67] accept also HF electric-fields as input working parameter, and MultiBolt [68, 69] includes a multi-harmonic model for intense microwave and terahertz excited LTPs [70]. However, none of these tools is directly prepared to describe the electron kinetics in a plasma excited by a time-dependent

electric-field pulse, because they assume a stationary isotropic component of the electron distribution function, and/or they adopt a Fourier time-expansion for a periodic excitation at given oscillating frequency ω.

In this work, we have extended the original capabilities of the LisbOn KInetics Boltzmann solver (LoKI-B) in order to obtain the solution of the EBE for plasmas excited by time-dependent (non-oscillatory, $\omega = 0$) electric fields. The updated simulation tool, to be available as open-source code [71], is used to analyse the temporal evolution of the electron kinetics, in plasmas excited by applying electric-field pulses to a stationary neutral gaseous background. No coupling with a chemistry model is done, hence the applied electric-fields are imposed with no self-consistent determination. By comparing the solutions of the EBE, when adopting a time-dependent formulation or a quasi-stationary description, it is possible to put forward the limitations of the latter approach, also clarifying the time intervals when it is expected to fail. Although limited to the electron kinetics behaviour, not considering the effects of heavy-particle interactions nor the time evolution of their densities, the analysis is pertinent and perfectly aligned with the preoccupations of recent similar studies [13].

The organisation of this paper is the following. Section 2 presents the time-dependent form and the solution method adopted in LoKI-B for the EBE. Section 3 compares results obtained with LoKI-B in dry air (80% N_2: 20% O_2), under the action of different electric-field pulses $E(t)$, when adopting a time-dependent formulation or a quasi-stationary approach. The study starts by considering the effects of step-fields (characterised by on-times $\tau_{on} \to \infty$) with different rise-times τ_{rise} (from 0 to 1 μs), and continues by analysing the response of the electrons to typical discharge pulses at limited τ_{on}'s, varying the rise-times between the ns and the μs scales. The analysis focuses on the time evolution of the EEDF, the electron power gained/lost in the various channels available, and some relevant electron swarm parameters. Section 4 concludes with final remarks.

2. The time-dependent electron Boltzmann equation

LoKI-B [67] is an open-source simulation tool initially developed to solve a time and space independent form of the two-term EBE, for non-magnetised non-equilibrium LTPs excited by DC/HF electric fields from different gases or gas mixtures. The tool gives a microscopic description of the electron kinetics, calculating the EEDF and several related macroscopic quantities, such as electron rate coefficients, transport parameters and power densities. LoKI-B accounts for variations in the number of electrons due to non-conservative events (ionisation and attachment) by assuming either a space-homogeneous exponential temporal growth or a time-constant exponential spatial growth of the electron density. The current version of LoKI-B considers binary collisions only, thus it does not include three-body dielectronic recombination events in the collisional operator. Note, however, that this can be a relevant loss mechanism in electropositive gases (such as nitrogen) at low pressure [72].

In this work, and following previous efforts of our research group on the same subject [37, 38], the original capabilities of LoKI-B have been extended in order to obtain the solution of the EBE for plasmas under the action of a time-dependent (non-oscillatory, $\omega = 0$) electric field. In this case, the electron velocity distribution function $\widetilde{F}(\vec{v}, t)$ can be expanded in Legendre polynomials with respect to the velocity $\vec{v}$

$$\widetilde{F}(\vec{v}, t) = \widetilde{F}(v, t) + \widetilde{F}^1(v, t)\cos\,\theta, \tag{1a}$$

and the resulting expression can be written in energy space, further separating the temporal evolution of the electron density $n_e(t)$, as follows

$$F(u, \cos(\theta), t) = n_e(t)\left[f(u, t) + f^1(u, t)\cos\,\theta\right], \tag{1b}$$

where $u = m_e v^2/(2e)$ is the electron kinetic energy in eV (with e and m_e the electron charge and mass, respectively); $f(u, t)$ and $f^1(u, t)$ are the isotropic component and the first anisotropic component of the electron distribution function, respectively, the former corresponding to the EEDF normalised so as to satisfy $\int_0^\infty f(u, t)\sqrt{u}\mathrm{d}u = 1$; and $\cos\theta$ corresponds to the Legendre polynomial of order one $P_1(\cos\theta)$, where θ is the polar angle of the electron velocity vector. We further assume an exponential temporal growth of the electron density with rate constant $\langle\nu_{eff}\rangle(t) \equiv \langle\nu_{ion}\rangle(t) - \langle\nu_{att}\rangle(t)$, corresponding to the net creation frequency of electrons due to non-conservative collisional mechanisms in the system under study

$$\frac{\mathrm{d}n_e(t)}{\mathrm{d}t} = \langle\nu_{eff}\rangle(t)\, n_e(t) \Rightarrow n_e(t) = n_0 e^{\int_0^t \langle\nu_{eff}\rangle(t')\,\mathrm{d}t'}, \tag{2}$$

$\langle\nu_{ion}\rangle$ and $\langle\nu_{att}\rangle$ being the electron mean frequencies for ionisation and attachment, respectively, and n_0 corresponding to the initial value of the electron density.

Under the previous conditions the EBE writes:

$$\frac{1}{N}\sqrt{\frac{m_e}{2e}}\sqrt{u}\frac{\partial f(u,t)}{\partial t} + \sqrt{\frac{m_e}{2eu}}\frac{\langle\nu_{eff}\rangle(t)}{N}uf(u,t) + \frac{1}{N}\sqrt{\frac{m_e}{2e}}\frac{\partial G(u,t)}{\partial u} = S(u,t) \tag{3a}$$

$$f^1(u,t) = -\frac{(E(t)/N)}{\Omega_c(u,t)}\frac{\partial f(u,t)}{\partial u}, \tag{3b}$$

where $N = p/k_B T_g$ is the density of the neutral background gas, at pressure p and temperature T_g (with k_B the Boltzmann constant); $G(u, t)$ is the *upflux function* [73], embedding information on the power gain/loss contributions due to continuous phenomena (e.g. the action of the applied electric field, the electron–neutral elastic collisions, the electron–electron Coulomb collisions, etc); $S(u, t)$ is the discrete collision operator that contains power loss/gain contributions due to inelastic/superelastic mechanisms, ionisation and attachment. The detailed expressions of G and S can be found in [67]; and

$$\Omega_c(u,t) \equiv \sigma_c(u) + \sqrt{\frac{m_e}{2eu}}\frac{1}{Nn_e(t)}\frac{dn_e(t)}{dt} = \sigma_c(u) + \sqrt{\frac{m_e}{2eu}}\frac{\langle\nu_{eff}\rangle(t)}{N}, \tag{4}$$

with $\sigma_c(u) \simeq \sum_k \chi_k \left\{ \sigma_{k,c}^{el}(u) + \sum_{i,j>i} \left[\xi_{k_i} \sigma_k^{(i,j)}(u) + \xi_{k_j} \sigma_k^{(j,i)}(u) \right] \right\}$ the electron–neutral *total* momentum-transfer cross section, where χ_k is the fraction of gas k in the mixture; ξ_{k_i}, ξ_{k_j} are the populations of target states i and j with gas k; $\sigma_{k,c}^{el}(u)$ is the electron–neutral *elastic* momentum-transfer cross section of gas k; and $\sigma_k^{(i,j)}(u)$, $\sigma_k^{(j,i)}(u)$ are the electron–neutral inelastic and superelastic cross sections of gas k for transitions $i \to j$ and $j \to i$, respectively (e.g. rotational and vibrational transitions). The quantity $\Omega_c(u,t)$ accounts for the changes in $f^1(u,t)$ due to (i) the transfer of momentum in all the collisional events (elastic, inelastic and superelastic; for the latter two, assuming isotropic scattering for lack of momentum-transfer data); and (ii) the time-evolution of the electron density, assuming an exponential growth, homogeneously distributed, with rate constant $\langle \nu_{eff} \rangle$. Note that it is possible to use (3b) to account for anisotropic scattering in inelastic/superelastic collisions, by resorting to momentum-transfer cross sections, self-consistently calculated from the corresponding differential cross sections. This approach was recently adopted to describe the anisotropic scattering in dipolar rotational collisions in CO [74]. Note also that the derivation of (3a) includes an additional expansion of the collision terms with respect to the small mass-ratio m_e/M_k (with M_k the mass of gas k in the mixture), truncated at 0th order for inelastic collisions and at first order for elastic collisions.

The isotropic equation (3a) is written considering an intrinsic time evolution for the EEDF, represented by the first term on its left-hand side (lhs), and a space-independent exponential temporal growth of the electron density due to the net effect of electron-impact ionisation and attachment, as described by the second term on the lhs of (3a), assuming that the electrons produced by ionisation and disappearing by attachment are homogeneously distributed. The anisotropic equation (3b) is written assuming a steady-state form, because the characteristic evolution time τ of the EEDF is much larger than the characteristic evolution time of the anisotropic component, i.e.

$$\tau \simeq \frac{1}{\sum_k \frac{m_e}{M_k} \nu_{k,c}^{el}} \gg \frac{1}{\nu_c} \simeq \frac{1}{\sum_k \nu_{k,c}^{el}}, \tag{5}$$

where ν_c is the electron–neutral total momentum-transfer collision frequency, which can usually be approximated by the corresponding elastic (cf (4)) $\sum_k \nu_{k,c}^{el} = \sum_k N_k \sqrt{2eu/m_e}\, \sigma_{k,c}^{el}$ (N_k being the density of gas k, such that $\sum_k N_k = N$). Thus, for momentum-transfer collision frequencies of the order of 10^{12} s^{-1} at atmospheric pressure, the present approximation is unable to describe the response of the electrons to variations of the electric field below the ps range.

Note that, despite the steady-state form of (3b), $f^1(u,t)$ is still time-dependent via the isotropic component $f(u,t)$, the electric field $E(t)$ and the quantity $\Omega_c(u,t)$. Therefore, the validity of the steady-state approximation is also to be checked against the rise time τ_{rise} of the applied electric field, holding only for $\tau_{rise} > 1/\sum_k \nu_{k,c}^{el}$. Note further that the inclusion of the time-dependent term in (3a) introduces a dependence of the EBE in the total gas density N, which is absent in the other terms of this equation (G/N and S are independent from N because they are exclusive functions of the electron-impact cross sections, and the reduced parameters E/N and ω/N). Therefore, the characteristic evolution times of the EEDF become a function of the degree of collisionality in the plasma, as suggested in (5) (see also section 3).

Multiplying (3a) by $\sqrt{2e/m_e}$ and integrating over all energies yields the electron continuity equation, per electron at unit gas density,

$$\frac{1}{N n_e(t)} \frac{dn_e(t)}{dt} = \frac{\langle \nu_{eff} \rangle(t)}{N} = \sqrt{\frac{2e}{m_e}} \int_0^\infty [S_{ion}(u,t) + S_{att}(u,t)]\, du, \tag{6}$$

which is automatically satisfied by calculating the net creation frequency from the cross sections used in the discrete collision operator $S(u,t)$, i.e. $\langle \nu_{eff} \rangle(t)/N = \sqrt{2e/m_e} \int_0^\infty [\sigma_{ion}(u) - \sigma_{att}(u)] f(u,t) u\, du$.

Multiplying (3a) by $u\sqrt{2e/m_e}$ and integrating over all energies yields the electron power balance equation, per electron at unit gas density,

$$\frac{\Theta(t)}{N} = \frac{\Theta_{growth}}{N} + \frac{\Theta_E}{N} + \frac{\Theta_{coll}}{N}, \tag{7}$$

where the term on the lhs $\Theta(t) \equiv d\varepsilon(t)/dt$ represents the intrinsic time evolution of the electron mean energy $\varepsilon(t) \equiv \int_0^\infty f(u,t) u^{3/2} du$ (this term is zero in stationary simulations), whereas the different terms on the right-hand side (rhs) represent, in order, the variation of the reduced power due to non-conservative mechanisms inducing a temporal net growth of the electron density, the reduced power gained from the applied electric field (positively defined, see [67]), and the reduced net power lost in collisional events (negatively defined, see [67]), leading to electronic, vibrational and rotational excitations/deexcitations. Note that, for interpretation purposes and comparatively to (3a), we kept only the intrinsic time-evolution term on the lhs of (7).

In LoKI-B, equations (3a) and (3b) are discretised in energy space adopting the finite differences scheme presented in [75]. The discretisation scheme is applied also to the integral expressions with the operator describing the temporal growth of the electron density, associated with non-conservative mechanisms, and the electron–electron collision operator. For the latter, the discretisation terms are further renormalised as detailed in [75], to ensure that the operator verifies standard properties, such as energy conservation and the correct Maxwellian behaviour for equilibrium conditions. As outcome, (3a) and (3b) are converted into a system of algebraic equations that can be integrated in time as an initial value problem. In matrix form this corresponds to

$$\frac{\partial f(t)}{\partial t} = C[f(t)] f(t), \tag{8}$$

where the non-linear features of matrix $C[f(t)]$ come from the operator describing the temporal growth of the electron density and/or the electron–electron collision operator. In particular, for each time t, the code evaluates iteratively the electron net creation frequency $\langle \nu_{eff} \rangle(t)$ and the electron–electron collision

upflux $G_{ee}(t)$, which are functions of $f(t)$ and, in the latter case, also of $n_e(t)$. When electron–electron collisions are included in the calculations, the time-dependent electron density depends on $\langle\nu_{eff}\rangle(t)$ through (2), which enhances the non-linearity of the problem. In this case, the system of equations (2) and (8) is solved using MATLAB's ordinary differential equation solver ode15s [76], given some initial conditions n_0 and $f(t=0) \equiv f_0$, for user-prescribed electric-field pulses, initial and final times, and sampling values of the field.

The solver adopts a variable-step, variable-order algorithm suited for stiff problems, based on a set of highly-stable implicit integration formulas of orders 1 to 5 (optionally, it can also use the backward differentiation formulas). The interest in adopting a stiff solver is because the integrator estimates the error at each iteration and then adjusts the timestep Δt to improve either the accuracy (i.e. by decreasing the timestep) or the efficiency (i.e. by increasing the timestep). At each time t the solution is updated using $f(t) = f(t-\Delta t) + (\partial f(t)/\partial t)\Delta t$ and $n_e(t) = n_e(t-\Delta t) + (dn_e(t)/dt)\Delta t$. The runtimes are very dependent on the working conditions, varying between 20–300 min on the single processor of a desktop computer, for relative tolerances $|f(t) - f(t-\Delta t)|/f(t-\Delta t) \simeq 10^{-6}$–$10^{-3}$ (depending on the user's choice), applied by the solver to adjust Δt for each instant t. At each t, the energy balance equation (7) is numerically calculated using the same matrix elements that result from the discretized EBE. Therefore the calculation of (7) is as accurate as the numerical solution of the EBE, ranging from $\sim$1% (for a time-dependent solution) to at least 10^{-10}% (in the quasi-stationary case, if the EBE is solved by direct matrix inversion).

3. Results and discussion

This section presents simulation results for the electron kinetics in dry air (80% N_2: 20% O_2) at room temperature and pressures 10^5 and 133 Pa (i.e. 760 and 1 Torr, respectively), excited by different electric-field pulses applied to a Maxwellian EEDF at $T_g = 300$ K as initial condition f_0. The results were obtained with LoKI-B, using the electron-scattering cross sections published at the IST-Lisbon database with LXCat for N_2 [77–80] and O_2 [81–84]. For ionisation, the energy sharing between the secondary and the scattered electrons adopts a differential cross section, normalized from available experimental data for the corresponding integral cross section, following the work of Opal *et al* [67, 85]. We have adopted the continuous approximation for rotations [86] to describe the electron-energy lost/gained in the excitation/deexcitation of rotational states, and considered inelastic/superelastic collisions with vibrational states by assuming Boltzmann distributions at 300 K for the VDFs of ground-states N_2 (X, v = 0–10) and O_2 (X, v = 0–4). Here, the focus is exclusively on the solution of the EBE, with no coupling to a chemistry model. Therefore, the VDFs considered are assumed to remain constant during the simulations.

The EBE was solved adopting either the time-dependent formulation given by equations (3a) and (3b) or a quasi-stationary approach, where the EBE assumes a time-independent form (i.e. with $\partial f/\partial t = 0$ in (3a), but keeping the temporal growth of the electron density if non-conservative mechanisms are considered), being solved for different values of the reduced electric-field over the duration of the pulse. In the latter case, the time evolution of the electron macroscopic parameters was deduced, first by evaluating a lookup table with 1000 values of E/N logarithmically separated in the range 0–55 Td, and then by linear interpolating the results obtained considering the particular time dependence of the electric field. The calculations adopted an energy grid with 1800 equidistant points and maximum energy $u_{max} = 18$ eV, ensuring a decrease of the EEDF of at least 10 decades (with respect to its maximum value). An alternative grid with 2200 points and $u_{max} = 22$ eV was also considered in some numerical tests, looking for possible changes in the results namely due to a better description of the ionisation mechanism; no significant modifications were observed.

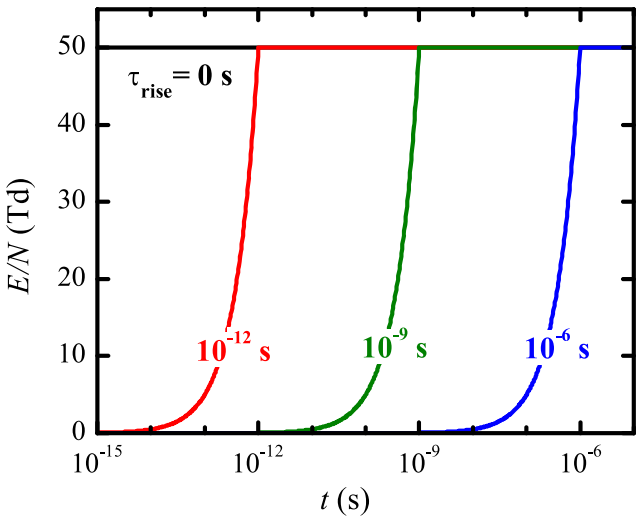

Figure 1. Time evolution of the reduced electric-fields given by (9) at $E_{max}/N = 50$ Td and for the following rise-times (in s): 0 (black curve), 10^{-12} (red), 10^{-9} (green), 10^{-6} (blue).

3.1. Results for step-reduced-fields

The response of the plasma electrons to a time-dependent excitation was first tested for atmospheric air, under the action of step-reduced-fields with the general form

$$\frac{E(t)}{N} = \begin{cases} \dfrac{E_{max}}{N}\dfrac{t}{\tau_{rise}}, & 0 \leqslant t \leqslant \tau_{rise} \\ \dfrac{E_{max}}{N}, & \tau_{rise} < t < \tau_{on} \to \infty \end{cases}, \qquad (9)$$

where we have considered $E_{max}/N = 50$ Td, and the rise-times $\tau_{rise} = 0, 10^{-12}, 10^{-9}, 10^{-6}$ s.

Figure 1 plots the time evolution of the reduced electric-fields given by (9), and figure 2 represents the corresponding time evolution of the electron mean energy, up to its final stationary value $\varepsilon_\infty = 1.23$ eV at $(E/N)_\infty = E_{max}/N = 50$ Td. The results in the latter figure allows concluding the following: (i) the natural response time of the electrons at atmospheric pressure is of the order of tens of picosecond, since

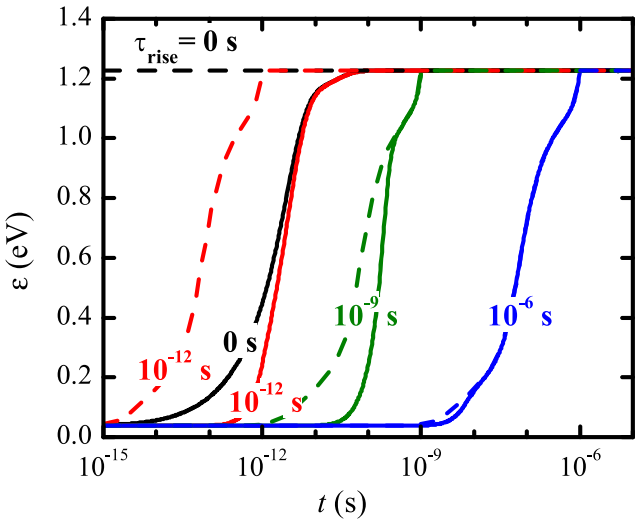

Figure 2. Time evolution of the electron mean energy, calculated with LoKI-B for dry-air plasmas at atmospheric pressure, adopting a time-dependent formulation (solid curves) or the quasi-stationary approach (dashed), for the same step-reduced-fields presented in figure 1.

$\varepsilon(t > 10^{-11}\ \text{s}) \simeq \varepsilon_\infty$ for $\tau_{\text{rise}} = 0$ s. This result is in agreement with direct Monte-Carlo simulations for similar conditions [87] and it shows that, at atmospheric pressure and for an instantaneous excitation, the electron kinetics can be solved for the stationary electric field if the analysis concerns evolution times beyond 10 ps; (ii) in general, the quasi-stationary approach holds for rise-times longer than the characteristic evolution time of the EEDF, i.e.

$$\tau_{\text{rise}} \gg \tau\ (\text{s}) \simeq \frac{5 \times 10^{17}}{N\ (\text{m}^{-3})}, \tag{10}$$

where the expression for τ was obtained from (5) assuming the typical value of $\nu^{\text{el}}_{k,\text{c}}/N \simeq 10^{-13}$ m^3 s^{-1} [88] and taking $m_\text{e}/M \simeq 2 \times 10^{-5}$ for dry air. At atmospheric pressure and room temperature, the criterion (10) gives $\tau_{\text{rise}} \gg 2 \times 10^{-8}$ s, thus confirming that the quasi-stationary approach holds for $\tau_{\text{rise}} = 1\ \mu$s, failing for $\tau_{\text{rise}} = 1$ ps and 1 ns.

As expected, the previous conclusions are confirmed also by the results for the time evolution of the EEDF (presented in figure 3) and of the reduced power, per electron at unit gas density, gained/lost in different phenomena (presented in figure 4). The latter figure separates the electron reduced power gained from the electric field, Θ_E/N, and lost to the different collisional channels considered: rotational, Θ_{rot}/N; vibrational, Θ_{vib}/N; and electronic, Θ_{ele}/N (see (7); note that $\Theta_{\text{rot}}/N + \Theta_{\text{vib}}/N + \Theta_{\text{ele}}/N \equiv -\Theta_{\text{coll}}/N$). Note also that figure 4 shows the electron power transfer at times where it takes values above the minimum of 10^{-20} eV m^3 s^{-1}, corresponding to a reasonable power density $\Theta_E n_\text{e} \sim 390$ W m^{-3} for a gas pressure $p = 10^5$ Pa, a gas temperature $T_\text{g} = 300$ K, and an electron density $n_\text{e} = 10^{16}$ m^{-3}. The results in figure 4 show that the quasi-stationary approach tends to enhance the relative importance of the different power loss channels (decreasing slightly that of the power gained from the electric field), especially during the early instants of the time evolution. In this case, the

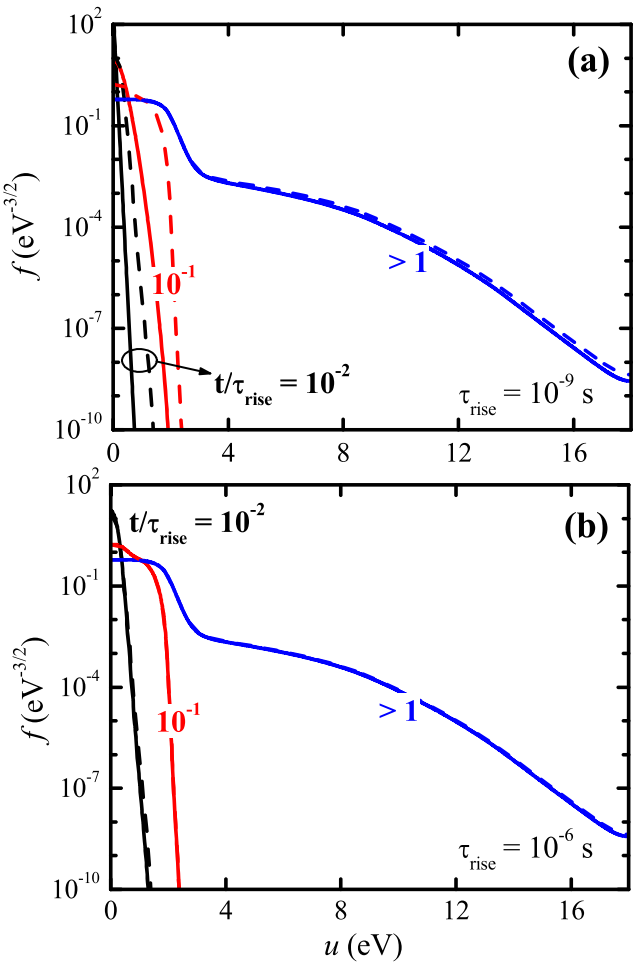

Figure 3. Time evolution of the EEDF, calculated with LoKI-B for dry-air plasmas at atmospheric pressure, for $t/\tau_{\text{rise}} = 10^{-2}$ (black curves), 10^{-1} (red) and > 1 (blue), adopting a time-dependent formulation (solid curves) or the quasi-stationary approach (dashed) for the step-reduced-fields presented in figure 1 with $\tau_{\text{rise}} = 10^{-9}$ s (a) and $\tau_{\text{rise}} = 10^{-6}$ s (b).

calculations impose a stationary power-balance at every time, satisfied by (7) with the lhs set to zero, i.e. ignoring the time evolution of the electron mean energy.

As confirmed by figures 3 and 4, the quasi-stationary approximation is particularly faulty at short times for $\tau_{\text{rise}} = 10^{-9}$ s $\ll \tau \simeq 2 \times 10^{-8}$ s, when the rise-time of the excitation field is much smaller than the characteristic evolution time of the EEDF; however, this approximation holds at longer times $t \gtrsim \tau_{\text{rise}}$, for which the plasma electrons have access to the full amount available of Joule power. As time advances, and thus the electric field increases, figure 4 shows the onsets of rotational, vibrational and electronic excitations, respectively, as expected considering the energy thresholds of these mechanisms. At shorter times the power losses are due mainly to rotational mechanisms, becoming controlled by vibrational mechanisms at longer times until steady-state, in which case $\Theta_E \simeq \Theta_{\text{vib}}$.

To conclude the analysis of simulations obtained for step-reduced-fields, figure 5 compares the time evolution of the EEDF and the first anisotropy adopting rise times of 10^{-12},

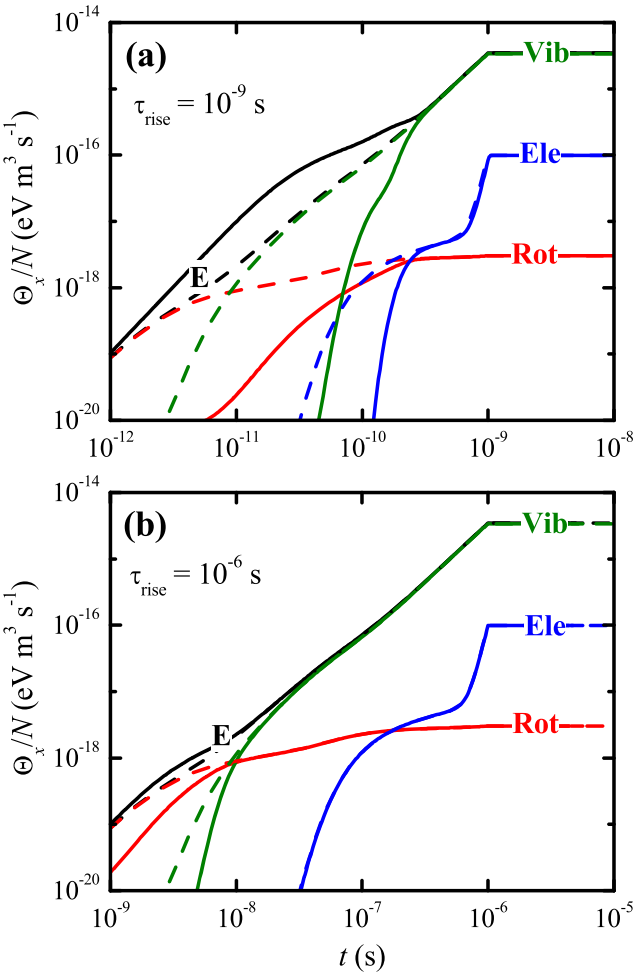

Figure 4. Time evolution of the electron power transfer per electron at unit gas density, Θ_x/N, calculated with LoKI-B for dry-air plasmas at atmospheric pressure, excited by the step-reduced-fields presented in figure 1 with $\tau_{\rm rise} = 10^{-9}$ s (a) and $\tau_{\rm rise} = 10^{-6}$ s (b), adopting a time-dependent formulation (solid curves) or the quasi-stationary approach (dashed). The colours are for the following power transfer channels: gain from the electric field ($x = E$, black); net loss in rotational excitations/deexcitations ($x =$ rot, red); net loss in vibrational excitations/deexcitations ($x =$ vib, green); loss in electronic excitations ($x =$ ele, blue).

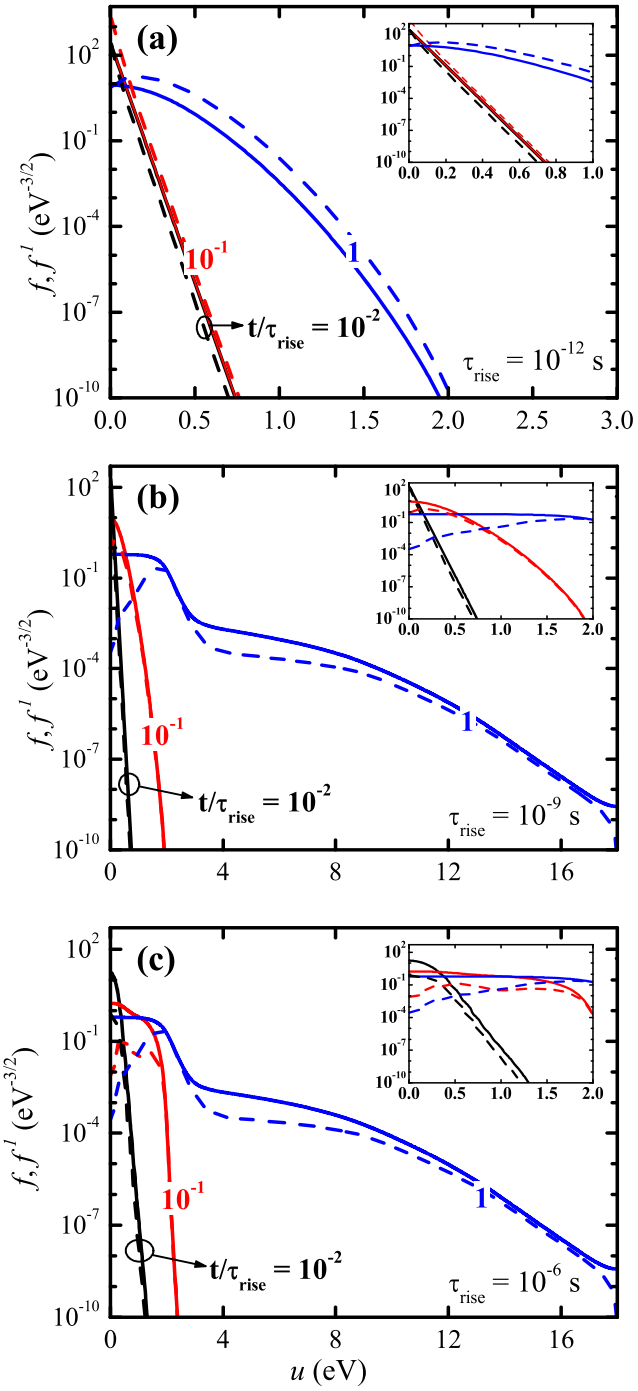

Figure 5. Time evolution of the EEDF (solid curves) and the first anisotropy (dashed), calculated with LoKI-B for dry-air plasmas at atmospheric pressure, for $t/\tau_{\rm rise} = 10^{-2}$ (black curves), 10^{-1} (red) and 1 (blue), adopting a time-dependent formulation for the step-reduced-fields presented in figure 1 with $\tau_{\rm rise} = 10^{-12}$ s (a), $\tau_{\rm rise} = 10^{-9}$ s (b) and $\tau_{\rm rise} = 10^{-6}$ s (c).

10^{-9} and 10^{-6} s. The results in this figure show that a fast variation in the electric field (e.g. for rise times of 1 ps or below) leads to a fast growing of the first anisotropy, causing $f^1 > f$ and compromising the two-term approximation. Moreover, the stationary approximation adopted here for f^1 is valid only if the time-variation of the electric field ($\tau_{\rm rise}$) is slower than the time required for the electrons to be in equilibrium with the local electric field ($1/\sum_k \nu^{\rm el}_{k,c}$), which corresponds to $\tau_{\rm rise} > 4 \times 10^{-13}$ s in this case. Thus, the calculation results at $\tau_{\rm rise} = 10^{-12}$ s (see figure 5(a)) are to be taken with extreme caution, since they are not fully within the validity conditions of the current framework. These conclusions agree with a similar temporal analysis presented in [44].

3.2. Results for reduced-field pulses

The response of the plasma electrons to a time-dependent excitation was further analysed for dry-air plasmas at pressures $p = 133$ and 10^5 Pa, subjected to reduced-field pulses with finite on-times $\tau_{\rm on} \simeq 10\tau_{\rm rise}$, given by the general expression

$$\frac{E(t)}{N}\,(\text{Td}) = \frac{E_0}{N}\sqrt{\frac{t}{\tau_{\rm rise}}}\,\exp\left(-\frac{t}{\tau_{\rm rise}}\right) \qquad (11)$$

and represented in figure 6. We have solved the EBE using LoKI-B for the reduced-field pulse (11) with $E_0/N = 100$ Td

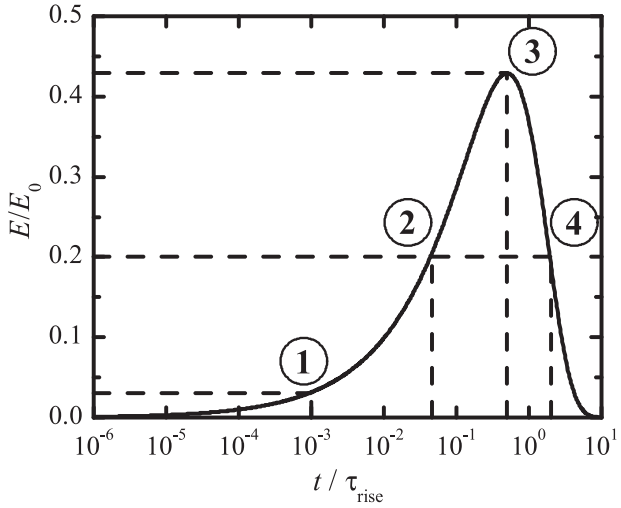

Figure 6. Relative intensity of the electric-field pulse (11), as a function of $t/\tau_{\rm rise}$. The labels (1)–(4) signal the particular conditions where we have analysed the time evolution of the EEDF (see figures 7 and 8), corresponding to $t/\tau_{\rm rise} \simeq 10^{-3}, 4\times10^{-2}, 0.5$ and 2, respectively.

and the two working pressures considered, adopting either a time-dependent formulation or a quasi-stationary approach. The solutions for the EEDF, at the four particular conditions (1)–(4) signalled in figure 6, are shown in figures 7 and 8 for $\tau_{\rm rise} = 10^{-6}$ s and 10^{-9} s, respectively.

The results in these figures confirm the previous conclusions about the validity of the quasi-stationary approach. In figure 7, the quasi-stationary approach produces solutions similar to the time-dependent formulation for $\tau_{\rm rise} \simeq 10^{-6}$ s $\gg \tau \simeq 2\times10^{-8}$ s in the high-collisionality situation ($p = 10^5$ Pa) [89], but predicts an evolution faster than that given by the time-dependent formulation for $\tau_{\rm rise} \simeq 10^{-6}$ s $\ll \tau \simeq 2\times10^{-5}$ s in the low-collisionality situation ($p = 133$ Pa) [90]. Note that the previous conclusions apply also to the electric-field falling region. For example, at low pressure both descriptions are able to yield similar solutions around the quasi-stationary (maximum) value of the electric field $E(t \simeq 10^{-6}\ {\rm s})/N$, but at later times a slightly divergence is again observed since $\tau_{\rm fall} \simeq 10^{-5}$ s $< \tau \simeq 2\times10^{-5}$ s. At faster rise times, e.g. for nanosecond pulses, figure 8 shows that it is not possible to satisfy the criterion (10) for the pressures considered here, since $\tau_{\rm rise} = 10^{-9}$ s $\ll \tau$ even at atmospheric pressure for which $\tau \simeq 2\times10^{-8}$ s. In this case, the time-dependent evolution of the EEDF is always slower than the predictions given by the quasi-stationary approach, a good agreement being achieved only at high pressure and around the maximum value of the reduced electric-field (see the lower graphs in the right-panel of figure 8).

The physical picture can be clarified by regarding the homogeneous EBE as a continuity equation in the (kinetic) energy space. Thus, during the time evolution, the electrons receive an energy flow from the electric field that does not instantly 'dissipate' into the gas through collisions, so the balance between these gain/loss flows translates into a slow temporal increase of the electron mean (kinetic) energy, similar to what is observed with the EEDF. This interpretation can be confirmed by analysing the electron power transfer as a function of time.

For the same reduced-field pulse (11) and working conditions ($E_0/N = 100$ Td; $\tau_{\rm rise} = 10^{-6}, 10^{-9}$ s; $p = 133, 10^5$ Pa), figure 9 shows the time evolution of the reduced power, per electron at unit gas density, gained/lost in the most relevant mechanisms considered here. As expected, the results in these figures confirm the observations and conclusions relative to the EEDF (cf figures 7 and 8), revealing additional features about the behaviour of the electron kinetics in time-dependent and quasi-stationary calculations. In particular: (i) for $\tau_{\rm rise} = 10^{-6}$ s the quasi-stationary approach holds for short relative times $t/\tau_{\rm rise} > 10^{-3}$ at high pressure, but only for much longer relative times $t/\tau_{\rm rise} \gtrsim 0.1$ at low pressure. In this case, at $p = 10^5$ Pa and in the fall part of the pulse at $t \simeq 10\tau_{\rm rise} = 10^{-5}$ s (see figure 9(b), right panel), it is possible to obtain a stationary situation corresponding to $\Theta_E \simeq \Theta_{\rm vib}$, even with time-dependent calculations; (ii) for $\tau_{\rm rise} = 10^{-9}$ s the predictions of the quasi-stationary approach are considerably different from those obtained in time-dependent calculations at low pressure, becoming comparable at atmospheric pressure only for $t/\tau_{\rm rise} \gtrsim 0.1$. In this case, however, the time-dependent predictions show that, even at 10^5 Pa and $t/\tau_{\rm rise} \simeq 10$ (see figure 9(a), right panel), the power transfer is still evolving according to $\Theta(t) \simeq \Theta_{\rm rot}$; (iii) usually, the quasi-stationary description yields a faster (and larger) power consumption in collisional processes, in line with the behaviour observed for the EEDF in figures 7 and 8. Moreover, in the extreme situation of a short pulse at low pressure (see figure 9(a), left panel), the evolution trends of the power lost in the various collisional channels are very different for both descriptions. Indeed, time-dependent calculations yield a larger maximum value of Θ_E/N (for $t/\tau_{\rm rise} \simeq 0.1$), thus revealing a strong unbalance between the power absorbed from the electric field and lost in collisions; at later times ($t/\tau_{\rm rise} \simeq 100$, long after the E/N peak) the time-dependent calculations still predict a large power lost in vibrational, rotational and electronic excitations, consistent with a slower decrease in the electron mean energy, whereas the quasi-stationary approach yields a balance between the power gained from the field and lost in vibrational excitations/deexcitations, i.e. $\Theta_E \simeq \Theta_{\rm vib}$; (iv) the similarity of the results obtained at long pulses/low pressures and short pulses/high pressures, for a scaling parameter $p\tau_{\rm rise} \simeq 10^{-4}$ Pa s (compare figure 9(b), left panel, with figure 9(a), right panel), confirms the role of the collisionality to obtain faster evolution times for the EEDF, as given by (10).

Note again that the previous analysis is exclusively for the behaviour of the EEDF as a result of electron-impact mechanisms. In particular, the present study does not take into account the effects of heavy-particle interactions, namely of vibrational–vibrational and vibrational–translation mechanisms, which can alter modelling predictions especially beyond the μs scale and/or in multi-pulse scenarios. Within these limitations, the analysis is relevant to control the description of the electron kinetics during the early times of an electric-field pulse, for example by monitoring the time evolution of the electron rate coefficients, which are key to

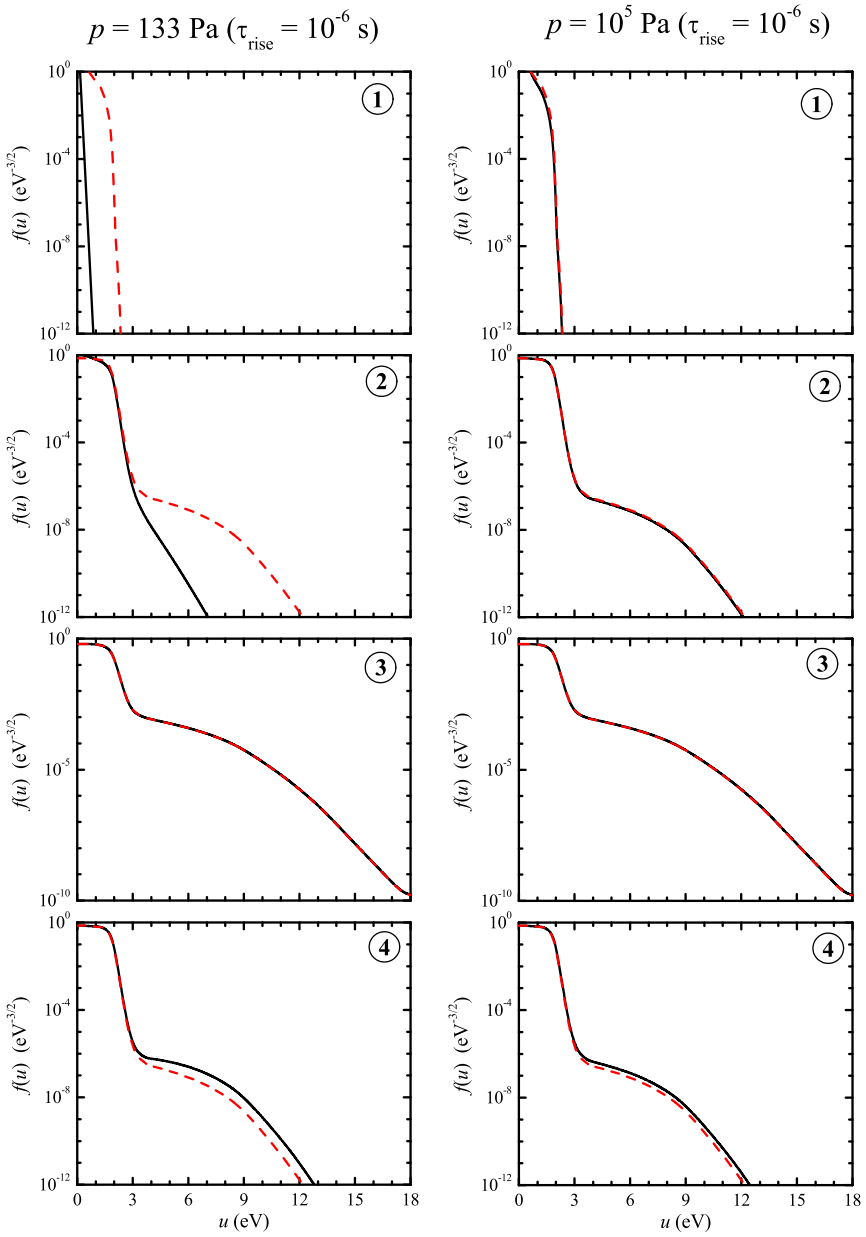

Figure 7. Time evolution of the EEDF, calculated with LoKI-B for dry-air plasmas, excited by the reduced-field pulse (11) with $E_0/N = 100$ Td and $\tau_{\rm rise} = 10^{-6}$ s, adopting a time-dependent formulation (solid black curves) or a quasi-stationary approach (red dashed). Left panel, results at low pressure $p = 133$ Pa; right panel, results at high pressure $p = 10^5$ Pa. In each panel, the four graphs were obtained at the (1)–(4) particular conditions signalled in figure 6.

obtain meaningful predictions in a time-dependent chemistry model.

As an example, figure 10 shows the time evolution of the ionisation rate coefficients for N_2 and for O_2, calculated under the same conditions as before: excitation of dry-air plasmas at atmospheric pressure, subjected to the electric-field pulse (11) with $E_0/N = 100$ Td and $\tau_{\rm rise} = 10^{-6}, 10^{-9}$ s, adopting a time-dependent formulation (to obtain $C_{\rm ion}(t)$) or a quasi-stationary approach (to obtain $C_{\rm ion}^{\rm stat}$). To help the comparison between the various calculations, the figure plots also the relative error $|\Delta C|/C_{\rm ion} \equiv |C_{\rm ion}(t) - C_{\rm ion}^{\rm stat}|/C_{\rm ion}(t)$. As expected from the results for the EEDF (cf figures 7 and 8), both approaches yield similar ionisation rate coefficients for $\tau_{\rm rise} = 10^{-6}$ s, in which case the electric field varies more slowly than the EEDF due to the high collisionality of the system, yet giving different values for $C_{\rm ion}(t)$ and $C_{\rm ion}^{\rm stat}$ when $\tau > \tau_{\rm rise} = 10^{-9}$ s. Note that, even in the most favorable scenario of $\tau_{\rm rise} = 10^{-6}$ s, the relative error is often close to unit, particularly in the early/late stages of the electric-field pulse. Note finally that similar observations and conclusions are obtained for other (excitation) rate coefficients, the main differences being related with the smaller/larger variation regions of the EEDF, according to the various thresholds of the excitation cross sections.

The previous results were obtained neglecting electron–electron collisions, but one might argue that their effect should

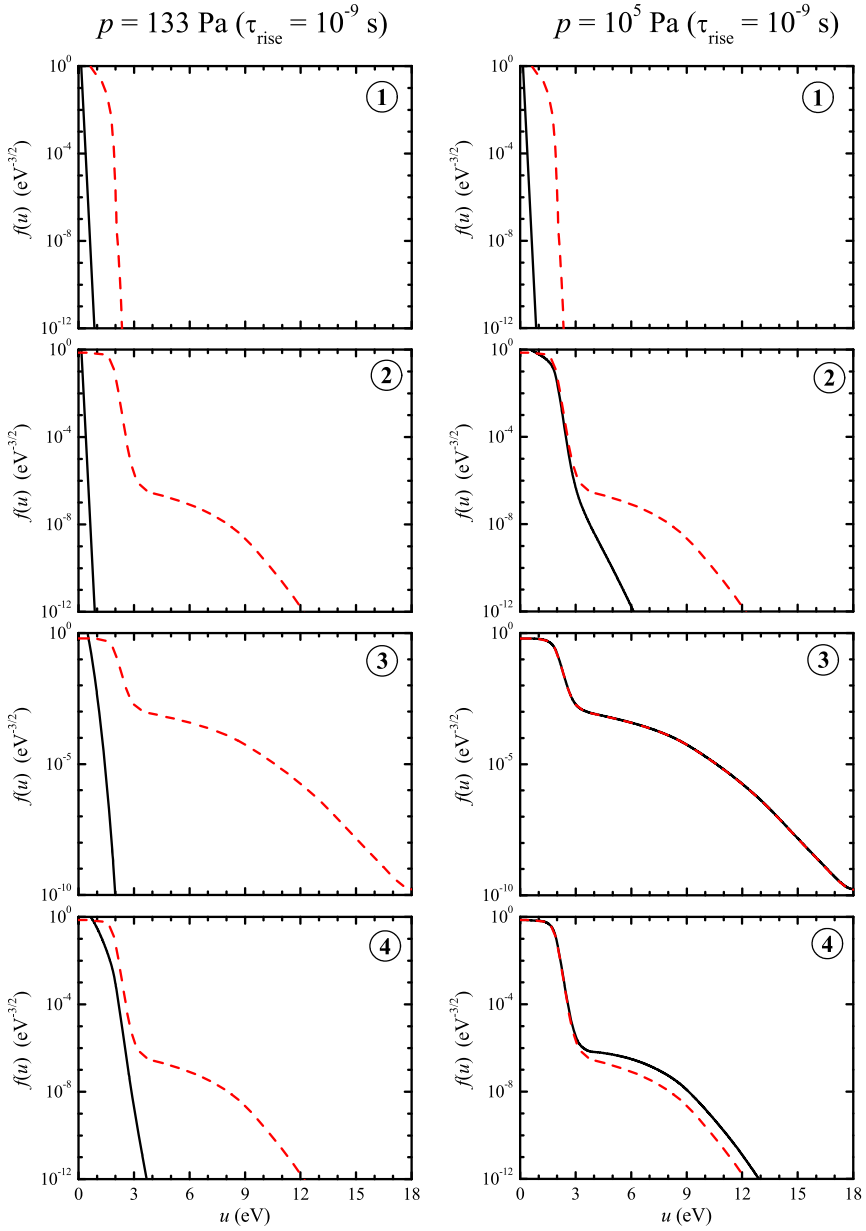

Figure 8. As in figure 7, but for $\tau_{\rm rise} = 10^{-9}$ s.

be also considered for an exponentially growing electron density, from an initial value n_0 according to (2). Self-consistent calculations considering a time-dependent electron density should be obtained in the broader context of a coupled solution with a chemistry model, extending the gains/losses of electrons to more phenomena than the ionisation/attachment considered in (2), such as heavy-particle interactions and transport to the walls. In any case, the technical handling of electron–electron collisions requires an update of $n_e(t)$ in the EBE, as described in section 2, regardless of the physical model adopted in the time evolution of the electron density.

We have tested the time-dependent version of LoKI-B also in the presence of electron–electron collisions, for N_2 at atmospheric pressure and room temperature, excited by an electric-field pulse (11) at rise-time $\tau_{\rm rise} = 10^{-9}$ s and amplitude E_0/N, applied to a Maxwellian EEDF at $T_g = 300$ K as initial condition f_0, and assuming a time-growing electron density from an initial value n_0, according to (2). As before, we have considered inelastic/superelastic collisions with vibrational states by assuming a Boltzmann distribution at 300 K for the VDF of ground-state N_2 (X, $v = 0$–10). In general, the influence of electron–electron collisions on the EEDF and the corresponding macroscopic parameters was found negligible for seed electron densities $n_0 \sim 10^9$ m^{-3} and typical $E_0/N \sim 100$ Td, thus we have pushed these quantities to larger (but still reasonable) values, in an attempt to obtain a visible effect. Figure 11 shows the time evolution of n_e and dn_e/dt, self-consistently obtained for $n_0 = 10^{19}$ m^{-3} and $E_0/N = 500$ Td by solving equations (3a) and (3b) together with (2). For the same conditions, figure 12 compares the time evolution of the electron mean energy, reduced mobility and ionisation rate coefficient, obtained neglecting or considering

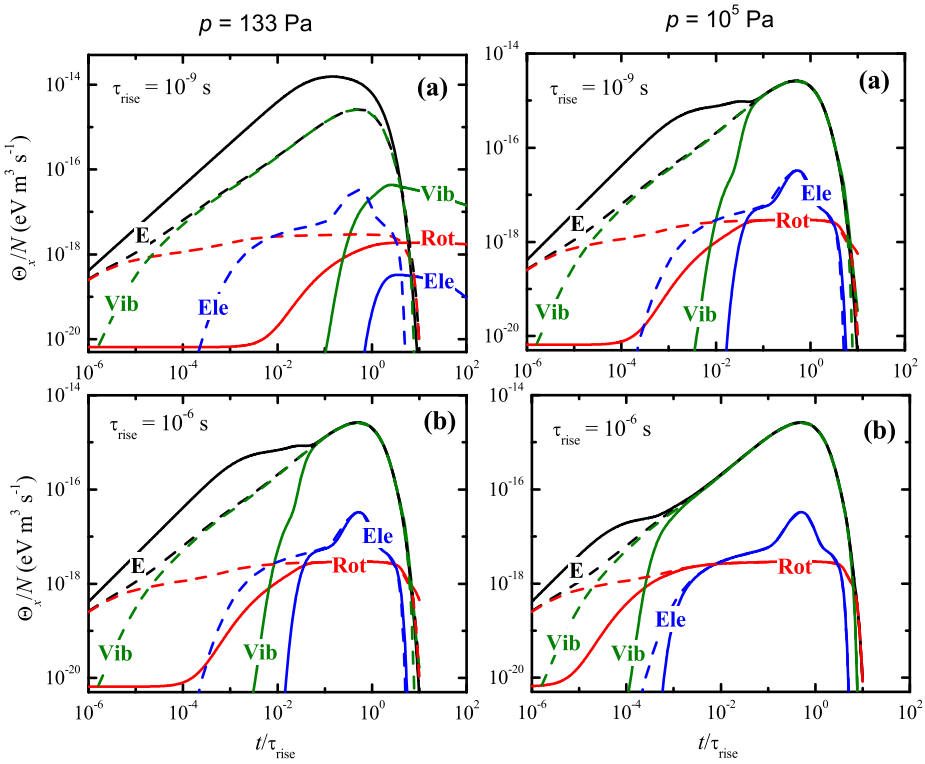

Figure 9. Time evolution (as a function of the relative time $t/\tau_{\rm rise}$) of the electron power transfer per electron at unit gas density, Θ_x/N, calculated with LoKI-B for dry-air plasmas, excited by the reduced-field pulse presented in figure 6 with $E_0/N = 100$ Td and $\tau_{\rm rise} = 10^{-9}$ s (a) or $\tau_{\rm rise} = 10^{-6}$ s (b), adopting a time-dependent formulation (solid curves) or the quasi-stationary approach (dashed), at $p = 133$ Pa (left panel) and 10^5 Pa (right panel). The colours are for the following power transfer channels: gain from the electric field ($x = E$, black); net loss in rotational excitations/deexcitations ($x =$ rot, red); net loss in vibrational excitations/deexcitations ($x =$ vib, green); loss in electronic excitations ($x =$ ele, blue).

electron–electron collisions, and in the latter case disregarding or including an exponential temporal growth for the electron density. The increase in the electron density observed in figure 11 is mainly due to the larger E_0/N value considered, which ensures ionisation rate coefficients that sustain the exponential building up of $n_{\rm e}(t)$, indeed $\langle\nu_{\rm ion}\rangle\tau_{\rm rise} \sim NC_{\rm ion}\tau_{\rm rise} \simeq 1$ yielding $C_{\rm ion} \sim 4 \times 10^{-17}$ m^3 s^{-1} for the working conditions adopted here (cf values in figure 12(c)). However, even with an exponential increase in $n_{\rm e}(t)$ between 10^{19} m^{-3} and $\sim 2.5 \times 10^{20}$ m^{-3}, the effect of electron–electron collisions remains negligible due to the low ionization degrees $n_{\rm e}/N \simeq 4 \times 10^{-7}$–$10^{-5}$, as confirmed by the results of figure 12. A small influence is noticeable only at later times, when the electron density attains the maximum value of its exponential growth and the electric-field pulse is close to extinction, and especially for μN, which depends on the energy-derivative of the EEDF. Note that similar results are obtained at lower pressures and electron densities, compliant with the same values of the scaling parameters $p\tau_{\rm rise} = 10^{-4}$ (yielding the same $C_{\rm ion} \sim 4 \times 10^{-17}$ m^3 s^{-1}) and $n_{\rm e}/N \simeq 4 \times 10^{-7}$–$10^{-5}$ (corresponding to $n_0 = 1.3 \times 10^{16}$ m^{-3} at $p = 133$ Pa).

4. Final remarks

In this work, we have analysed the temporal evolution of the electron kinetics in dry-air plasmas (80% N_2: 20% O_2), excited by electric-field pulses applied to a stationary neutral gaseous background at pressures $p = 10^5$, 133 Pa and temperature $T_{\rm g} = 300$ K. The electron kinetics was studied by solving the EBE (with no self-consistent coupling to a chemistry model) adopting either (i) a time-dependent formulation that considers an intrinsic time evolution for the EEDF, assuming the classical two-term expansion and a space-independent exponential temporal growth of the electron density; or (ii) a quasi-stationary approach, where the time-independent form of the EBE is solved for different values of the reduced electric-field over the duration of the pulse. The EBE was solved using the LoKI-B, whose original capabilities were extended to accept time-dependent non-oscillatory electric fields as input data.

The paper builds on previous work from different authors, duly recognized in section 1, with two main goals: (i) highlighting the limitations of the quasi-stationary approach, in obtaining a pseudo-time-dependent description of the electron kinetics in pulsed plasmas; (ii) delivering an updated version of the open-source code LoKI-B, addressing the intrinsic time evolution of the EEDF, for the benefit of the LTPs community.

The formulation adopted here involves two major approximations that should be highlighted. First, we have assumed that the anisotropic component of the electron distribution function remains in steady-state during the simulations, because

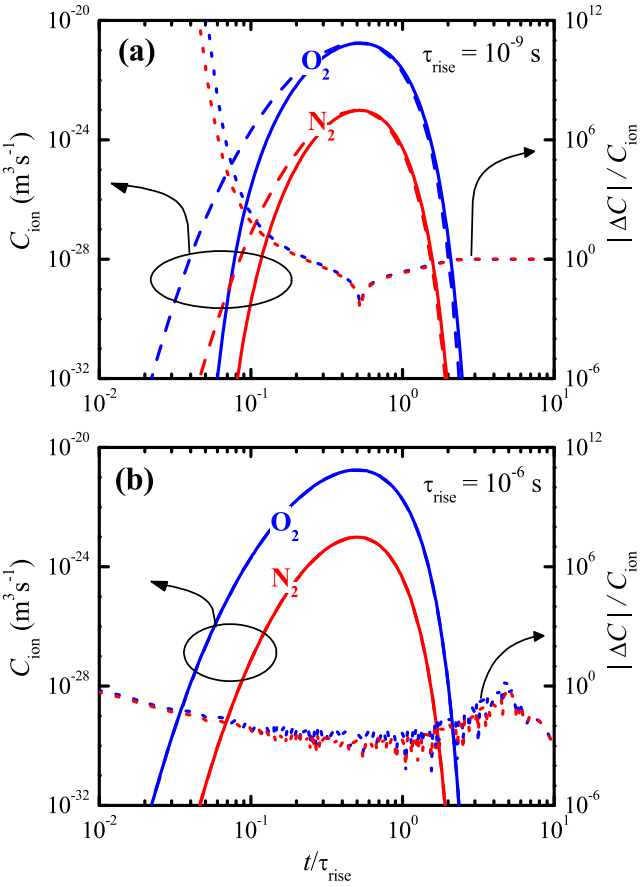

Figure 10. Time evolution (as a function of $t/\tau_{\rm rise}$) of the ionisation rate coefficients for O_2 (blue curves) and for N_2 (red), calculated with LoKI-B for dry-air plasmas at atmospheric pressure excited by the reduced-field pulse presented in figure 6 with $E_0/N = 100$ Td and $\tau_{\rm rise} = 10^{-9}$ s (a) or $\tau_{\rm rise} = 10^{-6}$ s (b), adopting a time-dependent formulation (giving $C_{\rm ion}(t)$, solid lines) or a quasi-stationary approach (giving $C_{\rm ion}^{\rm stat}$, dashed). The dotted lines represent the relative error $|\Delta C|/C_{\rm ion} \equiv |C_{\rm ion}(t) - C_{\rm ion}^{\rm stat}|\,/C_{\rm ion}(t)$.

its time evolution is much faster than that of the EEDF, given by the characteristic evolution time τ. Although the assumption is confirmed by (5), this equation also shows that the characteristic evolution time of the anisotropic component is of the order of $1/\nu_{k,c}^{\rm el} \simeq 10^{13}/N \simeq 4\times10^{-13}$ s, for air at atmospheric pressure, thus revealing that caution is advised when analysing results below the ps range, within the present framework. Second, we have considered a space-independent form of the EBE, which can be questioned in the modelling of discharge plasmas, where transient features induced by time-dependent excitations might trigger local space-time phenomena [44].

Within these approximations, LoKI-B was used to study the response of the plasma electrons to (i) step-reduced-fields with infinite on-times and rise-times $\tau_{\rm rise} = 0, 10^{-12}, 10^{-9}, 10^{-6}$ s, at atmospheric pressure; (ii) reduced-field pulses with finite on-times $\tau_{\rm on} \simeq 10\tau_{\rm rise}$ (for $\tau_{\rm rise} = 10^{-9}, 10^{-6}$ s), at $p = 10^5, 133$ Pa. The simulations show that the quasi-stationary approach gives solutions similar to the time-dependent formulation for rise-times longer than the characteristic evolution

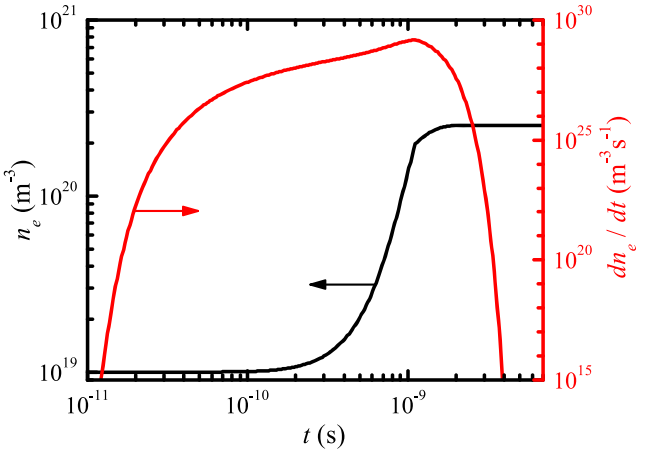

Figure 11. Time evolution of the electron density (black curve) and the time-derivative of the electron density (red), self-consistently obtained solving equations (2), (3a) and (3b), for N_2 at atmospheric pressure and room temperature, excited by the reduced-field pulse presented in figure 6 with $E_0/N = 500$ Td and $\tau_{\rm rise} = 10^{-9}$ s, and assuming an initial electron density $n_0 = 10^{19}$ m^{-3}.

time of the EEDF, i.e.

$$\tau_{\rm rise} \gg \tau\ ({\rm s}) \simeq \frac{5\times10^{17}}{N\ ({\rm m}^{-3})} \simeq \begin{cases} 2\times10^{-8}\ {\rm s}\ \ {\rm at}\ p = 10^5\ {\rm Pa},\ T_{\rm g} = 300\ {\rm K} \\ 2\times10^{-5}\ {\rm s}\ \ {\rm at}\ p = 133\ {\rm Pa},\ T_{\rm g} = 300\ {\rm K} \end{cases}, \quad (12)$$

meaning that a quasi-stationary description holds in a high-collisionality situation and long rise-times (e.g. microsecond pulses at atmospheric pressure), failing for faster rise-times (e.g. nanosecond pulses for both pressures considered here). In the latter cases, the time-dependent evolution of the EEDF is always slower than the quasi-stationary predictions, the deviations increasing for decreasing p and/or $\tau_{\rm rise}$. This result agrees also with observations of the time evolution of the reduced power gained/lost by the electrons, per electron at unit gas density. In particular, because the quasi-stationary description disregards the time evolution of the electron mean energy, it tends to enhance the relative importance of the power lost (decreasing slightly that of the power gained), thus preventing the unbalance between a fast power absorption from the field and a slow power consumption in collisional processes. Again, the situation becomes worse at short rise-times and/or low pressures. Moreover, the role of the collisionality to obtain faster evolution times for the electron kinetics is confirmed by the similar results obtained at long pulses/low pressures and short pulses/high pressures, as predicted by (12). This observation opens the way to an optimisation of the pulse duration depending on the gas pressure, as to maximize the energy absorption by the electrons.

We have also analysed the role of electron–electron collisions in time-dependent simulations (considering an exponentially growing electron density in time), for N_2 at atmospheric pressure and room temperature, excited by an electric-field pulse (11) at rise-time $\tau_{\rm rise} = 10^{-9}$ s and amplitude E_0/N.

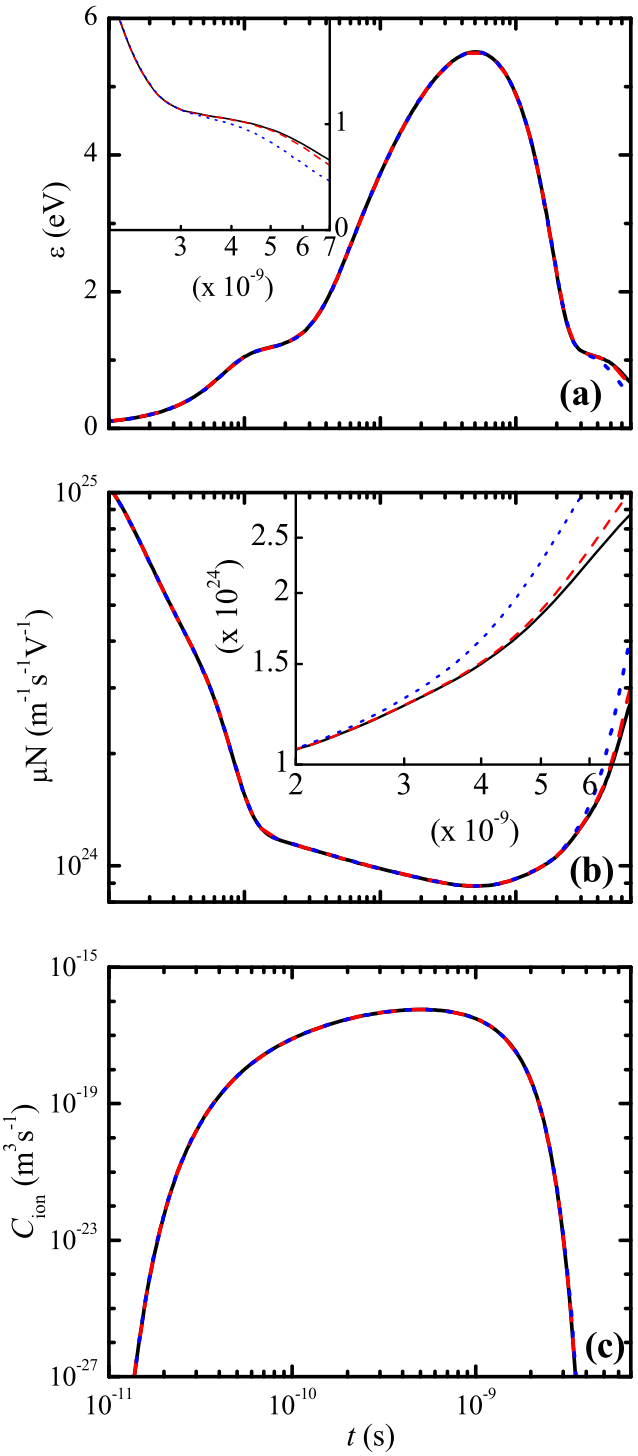

Figure 12. Time evolution of the electron mean energy (a), the electron reduced mobility (b) and the electron ionisation rate coefficient (c), calculated with LoKI-B for N_2 plasmas excited under the same conditions of figure 11, neglecting electron–electron collisions (black solid curves), considering electron–electron collisions at constant $n_e(t) = n_0$ (red dashed), and considering electron–electron collisions with $n_e(t)$ varying as shown in figure 11 (blue doted). The inserts in (a) and (b) are zooms over the 1–7 ns region.

For the working conditions considered, we concluded that the influence of this mechanism on the EEDF and the corresponding macroscopic parameters is negligible even for electron densities $n_0 \sim 10^{19}$ m^{-3} and $E_0/N \sim 500$ Td, due to the low values of both the ionisation degree and the ionisation rate coefficient.

This work focussed exclusively on the behaviour of the time-dependent EEDF as a result of electron-impact mechanisms. In particular, the present study did not take into account the effects of heavy-particle interactions, namely of vibrational–vibrational and vibrational–translation mechanisms, nor the time evolution of the heavy-particle densities, which can alter modelling predictions especially beyond the μs scale and/or in multi-pulse scenarios. Anyway, we do not expect relevant evolutions in the populations of rotational/vibrational states, nor in the gas temperature, for single pulse excitations with characteristic times $\tau_{rise} < 10^{-6}$ s. For example, in some systems, the gas temperature starts to be affected only after $\sim$10 μs, due to the energy-transfer from electrons to electronic excited states (and subsequent transfer to the translational energy modes of the gas), receiving the contribution of changes in the populations of rotational/vibrational states at even later times, beyond $\sim$0.1 ms [91]. Even with the previous limitations, we have shown that time-dependent rate coefficients (e.g. for electron-impact ionisation), calculated from the EEDFs obtained adopting the quasi-stationary approach, can be quite different than those obtained for a time-dependent solution of the EBE. As expected, the deviations become significant at low pressures and/or short rise-times, in particular for $\tau_{rise} = 10^{-9}$ s even at $p = 10^5$ Pa, which can have serious impact when describing the electron-impact mechanisms in a chemistry model as a function of time. In these cases, the description of the electrons and heavy-particles kinetics should adopt fully-coupled time-dependent Boltzmann-chemistry solvers [6, 13, 54], but as mentioned in section 1, the number of works using this approach remains relatively scarce. The updated time-dependent version of LoKI-B will be released as open-source code, thus facilitating its use in the modelling of time-dependent chemistries in LTPs. Work is in progress to develop an integrated time-dependent LoKI tool, coupling a Boltzmann and a chemistry solver.

Acknowledgments

This work was funded by Portuguese FCT—Fundação para a Ciência e a Tecnologia, under Projects UIDB/50010/2020 and UIDP/50010/2020. LLA received financial support from Grant SFRH/BSAB/150267/2019.

Data availability statement

The data that support the findings of this study are openly available at the following URL/DOI: http://www.lxcat.net/.

ORCID iDs

A Tejero-del-Caz https://orcid.org/0000-0002-9147-7909
V Guerra https://orcid.org/0000-0002-6878-6850
N Pinhão https://orcid.org/0000-0002-4185-2619
C D Pintassilgo https://orcid.org/0000-0003-1527-2976
L L Alves https://orcid.org/0000-0002-2677-574X

References

[1] Brandenburg R, Bruggeman P J and Starikovskaia S M 2017 *Plasma Sources Sci. Technol.* **26** 020201
[2] Samukawa S *et al* 2012 *J. Phys. D: Appl. Phys.* **45** 253001
[3] Starikovskaia S M 2006 *J. Phys. D: Appl. Phys.* **39** R265–99
[4] Popov N A 2016 *Plasma Sources Sci. Technol.* **25** 043002
[5] Klochko A V, Starikovskaia S M, Xiong Z and Kushner M J 2014 *J. Phys. D: Appl. Phys.* **47** 365202
[6] Colonna G, Laporta V, Celiberto R, Capitelli M and Tennyson J 2015 *Plasma Sources Sci. Technol.* **24** 035004
[7] Tholin F and Bourdon A 2013 *Plasma Sources Sci. Technol.* **46** 365205
[8] Rusterholtz D L, Lacoste D A, Stancu G D, Pai D Z and Laux C O 2013 *J. Phys. D: Appl. Phys.* **46** 464010
[9] Xu D A, Shneider M N, Lacoste D A and Laux C O 2014 *J. Phys. D: Appl. Phys.* **47** 235202
[10] Šimek M and Bonaventura Z 2018 *J. Phys. D: Appl. Phys.* **51** 504004
[11] Janda M, Hensel K and Machala Z 2018 *J. Phys. D: Appl. Phys.* **51** 334002
[12] Lepikhin N D, Popov N A and Starikovskaia S M 2018 *Plasma Sources Sci. Technol.* **27** 055005
[13] Colonna G, Laricchiuta A and Pietanza L D 2020 *Plasma Phys. Control. Fusion* **62** 014003
[14] Kobayashi S, Bonaventura Z, Tholin F, Popov N A and Bourdon A 2017 *Plasma Sources Sci. Technol.* **26** 075004
[15] Burnette D, Shkurenkov I, Adamovich I V and Lempert W R 2016 *Plasma Sources Sci. Technol.* **25** 025012
[16] Aleksandrov N L, Kindysheva S V and Kochetov I V 2014 *Plasma Sources Sci. Technol.* **23** 015017
[17] Adamovich I *et al* 2017 *Plasma Sources Sci. Technol.* **50** 323001
[18] Mei D, Zhu X, He Y-L, Yan J D and Tu X 2015 *Plasma Sources Sci. Technol.* **24** 015011
[19] Moss M S, Yanallah K, Allen R W K and Pontiga F 2017 *Plasma Sources Sci. Technol.* **26** 035009
[20] Zhang S, Gao Y, Sun H, Bai H, Wang R and Shao T 2018 *J. Phys. D: Appl. Phys.* **51** 274005
[21] Gao Y, Zhang S, Sun H, Wang R, Tu X and Shao T 2018 *Appl. Energy* **226** 534–45
[22] Scapinello M, Martini L M, Dilecce G and Tosi P 2016 *J. Phys. D: Appl. Phys.* **49** 075602
[23] Cheng H, Fan J, Zhang Y, Liu D and Ostrikov K 2020 *Catal. Today* **351** 103–12
[24] Sobota A, Guaitella O and Garcia-Caurel E 2013 *J. Phys. D: Appl. Phys.* **46** 372001
[25] Simeni M S, Goldberg B M, Zhang C, Frederickson K, Lempert W R and Adamovich I V 2017 *J. Phys. D: Appl. Phys.* **50** 184002
[26] Goldberg B M, Chng T L, Dogariu A and Miles R B 2018 *Appl. Phys. Lett.* **112** 064102
[27] Chng T L, Brisset A, Jeanney P, Starikovskaia S M, Adamovich I V and Tardiveau P 2019 *Plasma Sources Sci. Technol.* **28** 09LT02
[28] Hofmans M and Sobota A 2019 *J. Appl. Phys.* **125** 043303
[29] Wilhelm J and Winkler R 1979 *J. Phys. Colloq.* **40** C7-251–C7-267
[30] Winkler R and Wilhelm J 1980 *Comput. Phys. Commun.* **20** 113–8
[31] Loffhagen D and Sigeneger F 2009 *Plasma Sources Sci. Technol.* **18** 034006
[32] Loffhagen D and Winkler R 1994 *J. Comput. Phys.* **112** 91–101
[33] Bräuer T, Gortchakov S, Loffhagen D, Pfau S and Winkler R 1997 *J. Phys. D: Appl. Phys.* **30** 3223–39
[34] Hübner M, Gortschakow S, Guaitella O, Marinov D, Rousseau A, Röpcke J and Loffhagen D 2016 *Plasma Sources Sci. Technol.* **25** 035005
[35] Loureiro J 1993 *Phys. Rev.* E **47** 1262–75
[36] Sá P A, Loureiro J and Ferreira C M 1994 *J. Phys. D: Appl. Phys.* **27** 1171–83
[37] Guerra V, Sá P A and Loureiro J 2001 *Phys. Rev.* E **63** 046404
[38] Guerra V, Dias F M, Loureiro J, Sá P A, Supiot P, Dupret C and Popov T 2003 *IEEE Trans. Plasma Sci.* **31** 542–51
[39] Raspopović Z, Sakadžić S, Petrović Z L and Makabe T 2000 *J. Phys. D: Appl. Phys.* **33** 1298–302
[40] White R D, Dujko S, Ness K F, Robson R E, Raspopović Z and Petrović Z L 2008 *J. Phys. D: Appl. Phys.* **41** 025206
[41] Loffhagen D, Winkler R and Donkó Z 2002 *Eur. Phys. J. Appl. Phys.* **18** 189–200
[42] Trunec D, Bonaventura Z and Nečas D 2006 *J. Phys. D: Appl. Phys.* **39** 2544–52
[43] Dyatko N A, Napartovich A P, Sakadžić S, Petrović Z L and Raspopović Z 2000 *J. Phys. D: Appl. Phys.* **33** 375–80
[44] Hoder T, Loffhagen D, Voráč J, Becker M M and Brandenburg R 2016 *Plasma Sources Sci. Technol.* **25** 025017
[45] Yuan C, Bogdanov E A, Eliseev S I and Kudryavtsev A A 2017 *Phys. Plasmas* **24** 073507
[46] Winkler R, Deutsch H, Wilhelm J and Wilke C 1984 *Beitr. Plasma Phys.* **24** 303–16
[47] Winkler R, Capitelli M, Dilonardo M, Gorse C and Wilhelm J 1986 *Plasma Chem. Plasma Process.* **6** 437–56
[48] Winkler R, Dilonardo M, Capitelli M and Wilhelm J 1987 *Plasma Chem. Plasma Process.* **7** 125–37
[49] Winkler R, Dilonardo M, Capitelli M and Wilhelm J 1987 *Plasma Chem. Plasma Process.* **7** 245–65
[50] Capitelli M, Celiberto R, Gorse C, Winkler R and Wilhelm J 1988 *J. Phys. D: Appl. Phys.* **21** 691–9
[51] Gorse C, Capitelli M and Ricard A 1985 *J. Chem. Phys.* **82** 1900–6
[52] Gorse C and Capitelli M 1987 *J. Appl. Phys.* **62** 4072–6
[53] Gorse C, Cacciatore M, Capitelli M, De Benedictis S and Dilecce G 1988 *Chem. Phys.* **119** 63–70
[54] Pietanza L D, Colonna G and Capitelli M 2020 *Phys. Plasmas* **27** 023513
[55] Carbone E A D, Schregel C-G and Czarnetzki U 2016 *Plasma Sources Sci. Technol.* **25** 054004
[56] Wang W, Berthelot A, Zhang Q and Bogaerts A 2018 *J. Phys. D: Appl. Phys.* **51** 204003
[57] Morgan W L and Penetrante B M 1990 *Comput. Phys. Commun.* **58** 127–52
[58] Luque Alejandro https://github.com/aluque/bolos (accessed on 16 May 2021)
[59] Rabie MohamedFranck Christian https://lxcat.net/download/METHES (accessed on 16 May 2021)
[60] Rabie M and Franck C M 2016 *Comput. Phys. Commun.* **203** 268–77
[61] Biagi Stephen http://magboltz.web.cern.ch/magboltz/ (accessed on 16 May 2021)
[62] Biagi S F 1999 *Nucl. Instrum. Methods Phys. Res.* A **421** 234–40
[63] Hagelaar Gerjan http://www.bolsig.laplace.univ-tlse.fr/ (accessed on 16 May 2021)
[64] Hagelaar G J M and Pitchford L C 2005 *Plasma Sources Sci. Technol.* **14** 722–33
[65] Dyatko N A, Kochetov I V, Napartovich A P and Sukharev A G 2015 EEDF: the software package for calculations of the electron energy distribution function in gas mixtures https://lxcat.net/download/EEDF/ (accessed on 16 May 2021)
[66] N-Plasmas Reactive: Modelling and Engineering (N-PRiME) https://nprime.tecnico.ulisboa.pt/loki/ (accessed on 16 05 2021)
[67] Tejero-del-Caz A, Guerra V, Gonçalves D, Lino da Silva M, Marques L, Pinhão N, Pintassilgo C D and Alves L L 2019 *Plasma Sources Sci. Technol.* **28** 043001

[68] Stephens Jacob https://gitlab.com/LXCatThirdParty/MultiBolt (accessed on 16 05 2021)
[69] Stephens J 2018 *J. Phys. D: Appl. Phys.* **51** 125203
[70] Stephens J C 2018 *Phys. Plasmas* **25** 103502
[71] N-Plasmas Reactive: Modelling and Engineering (N-PRiME) https://github.com/IST-Lisbon/LoKI (accessed on 16 05 2021)
[72] Colonna G and D'Angola A 2016 *Plasma Modeling Methods and Applications* (Bristol: IOP Publishing) ch 2
[73] Allis W P 1956 *Motions of ions and electrons Handbuck der Physik* vol 21 ed S Flügge (Berlin: Springer) pp 383–444
[74] Vialetto L, Ben Moussa A, van Dijk J, Longo S, Diomede P, Guerra V and Alves L L 2021 *Plasma Sources Sci. Technol.* submitted
[75] Rockwood S D 1973 *Phys. Rev.* A **8** 2348–58
[76] MathWorks *Matlab documentation webpage* https://mathworks.com/help/matlab/ref/ode15s.html (accessed on 16 May 2021)
[77] N_2 on IST-Lisbon database www.lxcat.net (accessed on November 2019)
[78] Loureiro J and Ferreira C M 1986 *J. Phys. D: Appl. Phys.* **19** 17–35
[79] Pitchford L C and Phelps A V 1982 *Bull. Am. Phys. Soc.* **27** 109
[80] Tachibana K and Phelps A V 1979 *J. Chem. Phys.* **71** 3544
[81] O_2 on IST-Lisbon database www.lxcat.net (accessed on November 2019)
[82] Gousset G, Ferreira C M, Pinheiro M, Sá P A, Touzeau M, Vialle M and Loureiro J 1991 *J. Phys. D: Appl. Phys.* **24** 290–300
[83] Alves L L, Coche P, Ridenti M A and Guerra V 2016 *Eur. Phys. J.* D **70** 124
[84] Phelps A V 1985 *Technical Report 28 JILA Information Center Report* University of Colorado Boulder, Colorado, USA
[85] Opal C B, Peterson W K and Beaty E C 1971 *J. Chem. Phys.* **55** 4100–6
[86] Ridenti M A, Alves L L, Guerra V and Amorim J 2015 *Plasma Sources Sci. Technol.* **24** 035002
[87] Moss G D, Pasko V P, Liu N and Veronis G 2006 *J. Geophys. Res.* **111** A02307
[88] Guerra V, Tejero-del-Caz A, Pintassilgo C D and Alves L L 2019 *Plasma Sources Sci. Technol.* **28** 073001
[89] Tejero-del-Caz Antonio https://youtube.com/watch?v=aCLfDSlgjds & feature=youtu.be (accessed on 16 May 2021)
[90] Tejero-del-Caz Antonio https://youtube.com/watch?v=QCJzLWc5W1M & feature=youtu.be (accessed on 16 May 2021)
[91] Colonna G 2020 *Plasma Sources Sci. Technol.* **29** 065008